Journal of Systems Engineering and Electronics
Vol. PP, No. 99, August 2025, pp.1 – 11

2D-DOA estimation for NLOS environments via intelligent reflecting surface

DUAN Min[1,2], LI Xiaopeng[1,2,*], HUANG Lei[1,2], HUA Meng[3], and LI Qiang[1,2]

1. State Key Laboratory of Radio Frequency Heterogeneous Integration, Shenzhen University, Shenzhen 518000, China;
2. College of Electronics and Information Engineering, Shenzhen University, Shenzhen 518000, China;
3. Department of Electrical and Electronic Engineering, Imperial College London, London SW72AZ, UK

Abstract: Direction-of-arrival (DOA) estimation provides the angle information about interesting targets for array radar systems. However, conventional algorithms are designed for line-of-sight (LOS) scenarios and thus cannot be used to estimate non-LOS (NLOS) targets. Recently, intelligent reflecting surface (IRS) has been applied to DOA estimation for NLOS environments. This paper proposes a geometric model utilizing IRS for DOA estimation in NLOS scenarios. First, we establish an IRS-aided DOA estimation framework, where one-pair-IRSs is used to manipulate the propagation direction of the detection signals. Then, we formulate the estimation task using the elliptic positioning technique. Subsequently, we derive a closed-form solution for the resultant problem. Furthermore, we improve the architecture using multi-pair-IRSs and then design a binary weighting method to enhance the accuracy of DOA estimation. In comparison with the existing methods, the proposed algorithm is able to estimate two-dimensional (2D) DOA for NLOS targets. Numerical simulations are conducted to validate the effectiveness of IRS for DOA estimation in NLOS environments.

Keywords: direction-of-arrival (DOA) estimation, non-line-of-sight (NLOS), intelligent reflecting surface, elliptic positioning, binary weighting.

DOI: 10.23919/JSEE.2025.000038

1. Introduction

Direction-of-arrival (DOA) estimation plays a crucial role in array radar systems as it provides the angular information about targets, which is vital for the overall performance of radar. Through DOA estimation, radar systems can significantly enhance the detection, positioning, and tracking capabilities, making them more effective in various applications [1]. Specifically, as an important component of defense informatization, DOA estimation has been widely applied in several military fields [2]. For instance, in military reconnaissance, DOA estimation helps determine the location and movement direction of enemy targets, providing critical information for tactical decision-making. In air defense and missile defense systems, accurate angular information aids in the fast identification and interception of incoming aerial threats. Additionally, DOA estimation is important for long-range early warning systems, enabling the early detection of potential threats and allowing more time for preventive measures. In a word, DOA estimation not only enhances the performance of array radar, but also provides essential support for various military applications, indicating that it is an indispensable part of modern defense technology [2].

A variety of estimation techniques have been developed to ascertain the DOA of interesting targets, including multiple signal classification (MUSIC) [3] and its variations [4–7], estimating signal parameter via rotational invariance techniques (ESPRIT) [8], and enhanced principal-singular-vector utilization for modal analysis (EPUMA) [9]. The aforementioned algorithms require targets satisfying the line-of-sight (LOS) conditions. However, in practice, array radar systems might be confronted with non-LOS (NLOS) environments, where the direct path between the transmitter (or receiver) and target is obstructed by physical objects [10]. Addressing NLOS-DOA estimation is pivotal for overcoming signal propagation challenges in such complicated environments. This technology holds immense significance in enhancing positioning precision, upgrading communication quality, bolstering radar detection capabilities, sup-

Manuscript received October 10, 2024.
*Corresponding author.
This work was supported by the National Natural Science Foundation of China (62401373; 62371306), the National Science Fund for Distinguished Young Scholars (61925108), the Key Project of International Cooperation and Exchanges of the National Natural Science Foundation of China (62220106009), the project of Shenzhen Peacock Plan Teams (KQTD20210811090051046), and the Research Team Cultivation Program of Shenzhen University (2023DFT003).

porting autonomous driving, intelligent transportation systems, and improving indoor navigation [11,12]. Given these complexities, conventional DOA estimation algorithms are insufficient for accurately estimating the DOAs of NLOS targets.

1.1 Related works

To tackle this challenge, several DOA estimation techniques have been developed, such as the deployment of multiple small cell base stations (SBSs) [13] and distributed multiple-input multiple-output (MIMO) radar systems [14]. The former increases the number of SBSs or expands the distance between them to transform NLOS scenarios into LOS environments. This not only enhances spectrum efficiency and reduces interference, but also improves overall communication efficiency. The latter establishes a multi-path echo model for ultra-wide-band MIMO radar. Then, the range-Doppler topology is exploited to design a multi-path recognition strategy to match the time of arrivals (TOAs) with different types of multi-paths and targets. Finally, the DOAs of NLOS targets are determined according to the recognition results.

On the other hand, intelligent reflecting surfaces (IRSs) have been widely studied in wireless communication and radar fields [15,16], e.g., the DOA estimation [17−19], indoor location [20,21], unmanned aerial vehicle communication systems [22−24], channel estimation [25−27] and so on. As IRSs are composed of numerous passive elements designed to manipulate electromagnetic signals, they can reconfigure the propagation properties of the wireless environment [28]. By intelligently controlling the reflection and propagation of electromagnetic waves, IRS can significantly enhance signal quality, coverage, and network capacity, while maintaining energy efficiency [29−32]. Therefore, IRSs have been considered as a promising tool for DOA estimation in NLOS scenarios by utilizing their characteristic, which can intelligently control the reflection signal paths [33,34]. For example, [35] considered a joint TOA and DOA estimation for localization and proposed a TOA/DOA estimator without iteration under the semi-passive IRS architecture. Reference [36] proposed exploiting multiple IRSs to create virtual LOS links between the base station and targets in communication systems. Then, an on-grid IRS beam scanning algorithm was designed to search for DOA. In [37], a polarized IRS architecture was devised to aid the two-dimensional (2D) DOA estimation for NLOS signals, where both IRS and base station (BS) are equipped with arbitrarily placed electromagnetic vector sensor arrays. It is worth mentioning that the estimated DOA is the angle between users and the IRS.

1.2 Motivations and contributions

In [35−37], IRSs are utilized to aid the DOA estimation. Both [35] and [36] employed the MUSIC algorithm for DOA estimation. The former utilizes the MUSIC to estimate the DOA of the IRS-target link, while the latter employs it to search for the DOA of the BS-target link. In addition, the localization in [36] requires joining the DOA estimation of the BS-Target via a LOS link and that of the IRS-Target. It is worth mentioning that the approach in [35] does not estimate the DOA of BS-Target via the NLOS link of BS-IRS-Target. The algorithm in [37] exploits the subspace estimation technique, whose performance severely degrades in low signal-to-noise ratios. In addition, this method cannot be used in the situation where the number of signal sources exceeds the number of array antennas. In addition, [37] explored the polarization characteristic of antenna to estimate DOA, while neglects the spatial feature of the array at the BS. This overlook leads to significant performance degradation and imposes limitations on system design.

To address the limitations of the existing DOA estimation method in NLOS environments, we propose an IRS-aided 2D-DOA estimation architecture for NLOS sources, where the transmission path of signals is reconfigured using IRSs. Consequently, a virtual LOS link between the NLOS target and antenna array is established. Then, we devise an efficient algorithm to seek the DOA based on the elliptic positioning (EP) technique [38]. As a result, the DOA estimate is calculated using a closed-form solution. Moreover, we exploit the multi-pair-IRSs to improve the estimation accuracy or extend the detection range. Furthermore, the eccentricity of the ellipse is adopted to design a binary weight method for the overall system performance enhancement. The key contributions of this study are summarized as follows:

(i) A novel one-pair-IRSs aided 2D-DOA estimation framework is established, where the characteristics of the signal transmission path can be changed.

(ii) An effective algorithm is devised based on the proposed estimation framework. We assume that the coordinates of antenna arrays and IRSs are known and then utilized to formulate the DOA estimation problem into an EP architecture. Then, a closed-form solution is derived for the resultant task.

(iii) A binary weighting (BW) approach is suggested for the multi-pair-IRSs aided DOA estimation that is designed to extend the detection zone or enhance the accuracy of DOA estimation.

1.3 Organization

The remainder of this paper is organized as follows. Section 2 introduces the system model of DOA estimation for NLOS sources. The estimation algorithm for the resultant task is presented in Section 3. Section 4 designs a multi-IRSs aided 2D-DOA estimation framework to improve the accuracy or expand the range of DOA estimation. Section 5 conducts numerical experiments to investigate the performance of the proposed methods. Finally, concluding remarks are given in Section 6.

2. Proposed system model

In this section, we present an IRS-aided DOA estimation model for NLOS environments.

2.1 One-pair-IRSs aided DOA estimation framework

As shown in Fig. 1, an interesting target is at the NLOS direction of the antenna array. To estimate its DOA, we introduce two IRSs to create a virtual LOS link between it and the antenna array. Specifically, IRS_1 reflects the detection signal from the transmitting antenna array (BS_e), while IRS_2 reflects the detection signal from the target and delivers it to the receiving antenna array (BS_r). As a result, the antenna array is able to detect the target. It is important to note that each IRS (denoted as IRS_m, where $m = 1,2$) is a uniform planar array (UPA) with N_s elements.

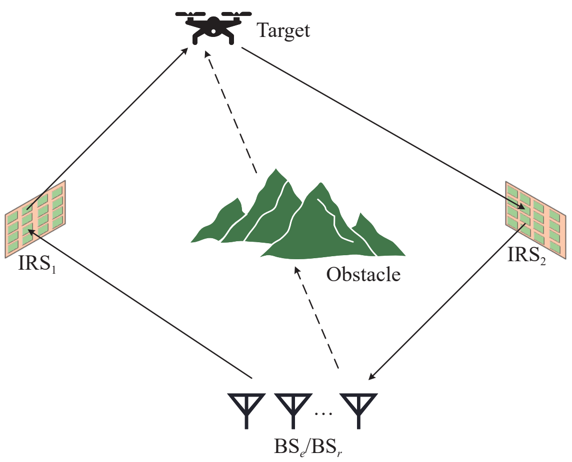

Fig. 1 One-pair-IRSs aided DOA estimation framework

2.2 Signal model

In this subsection, we introduce the signal model for the IRS-aided DOA estimation. First of all, the normalized LOS channels of antenna array-to-IRS and IRS-to-target are respectively defined [39] as

$$\begin{cases} \boldsymbol{h}_{\mathrm{B2S}} = [\mathrm{e}^{\mathrm{j}\psi_1^{\mathrm{bs}}}, \mathrm{e}^{\mathrm{j}\psi_2^{\mathrm{bs}}}, \cdots, \mathrm{e}^{\mathrm{j}\psi_{N_s}^{\mathrm{bs}}}]^{\mathrm{T}} \\ \boldsymbol{h}_{\mathrm{S2T}} = [\mathrm{e}^{\mathrm{j}\psi_1^{\mathrm{st}}}, \mathrm{e}^{\mathrm{j}\psi_2^{\mathrm{st}}}, \cdots, \mathrm{e}^{\mathrm{j}\psi_{N_s}^{\mathrm{st}}}]^{\mathrm{T}} \end{cases} \tag{1}$$

where ψ_i^{bs} and ψ_i^{st} $(i = 1,2,\cdots,N_s)$ denote the phase shift of the two channels, respectively.

In general, an IRS is composed of a large array of passive reflecting elements with a specially designed physical structure. Each reflecting element is controlled in a software-defined manner to change the reflection electromagnetic properties (e.g., the phase shift) of the incident radio frequency (RF) signals [40–42]. Therefore, IRS has the capability to control the angle-of-departure (AOD) of the reflected signal. Specifically, the reflection coefficient matrix of the IRS is defined as

$$\boldsymbol{\Phi} \triangleq \mathrm{diag}(\mathrm{e}^{\mathrm{j}\phi_1}, \mathrm{e}^{\mathrm{j}\phi_2}, \cdots, \mathrm{e}^{\mathrm{j}\phi_{N_s}}) \tag{2}$$

where ϕ_n is the phase shift of the nth element.

Given an incident signal $\boldsymbol{x} \in \mathbf{C}^{N_s}$ transmitted from BS_e, the signal reflected by IRS_1 is given [39] by

$$y_1 = \sqrt{\beta_S}\boldsymbol{h}_{\mathrm{S2T}}^{\mathrm{T}}\boldsymbol{\Phi}\boldsymbol{h}_{\mathrm{B2S}}x \tag{3}$$

where β_S is the path loss between the antenna array and the target. Note that the impact of noise is neglected in (3). This is because we utilize the IRS as a passive one in this paper.

Similarly, the detection signal through the target-IRS_2-BS_r link is expressed as

$$y_2 = \sqrt{\beta_S}\boldsymbol{h}_{\mathrm{S2T}}^{\mathrm{T}}\boldsymbol{\Phi}\boldsymbol{h}_{\mathrm{B2S}}y_1 \tag{4}$$

where y_2 denotes the signal reflected by IRS_2.

At the receiver, the antenna array is considered as a uniform linear array (ULA) with N_a antennas. Thereby, the array steering vector is defined as

$$\boldsymbol{a}(\theta_k) = \left[1, \mathrm{e}^{\mathrm{j}\frac{2\pi \cdot d\sin\theta_R}{\lambda}}, \cdots, \mathrm{e}^{\mathrm{j}\frac{2\pi(N_a-1)d\sin\theta_k}{\lambda}}\right]^{\mathrm{T}} \tag{5}$$

where λ is the carrier wavelength and θ_k denotes the angle of incident signal.

Finally, the received signal $\boldsymbol{y} \in \mathbf{C}^{N_a}$ at the receiver is represented as

$$\boldsymbol{y} = \boldsymbol{a}(\theta_k)y_2 + \boldsymbol{\epsilon} + \boldsymbol{n} \tag{6}$$

where $\boldsymbol{\epsilon} \in \mathbf{C}^{N_a}$ denotes the interference and $\boldsymbol{n} \in \mathbf{C}^{N_a}$ is the additive noise.

3. Proposed algorithm

In this section, based on the proposed system model, we devise an efficient algorithm to estimate 2D-DOA for a NLOS target by utilizing the EP technique. The signals received by the sensor array form an elliptical trajectory on a certain plane [43]. By computing the parameters of the ellipse, namely, center, major axis, minor axis, and focus, the position of the signal source is located and then the DOA can be estimated.

3.1 3D Cartesian coordinate system establishment

In this subsection, we establish a 3D Cartesian coordinate system, illustrated in Fig. 2. The locations of the

IRSs and antenna array are assumed to be known. Since the transmitting and receiving arrays are located adjacent to each other, they share the identical coordinates $B=(X_B,Y_B,Z_B)$. In addition, we denote the positions of IRS_1, IRS_2, and the target as $S_1=(0,0,0)$, $S_2=(X_{S_2},0,0)$, and $T=(\mathrm{X}_T,Y_T,Z_T)$, respectively.

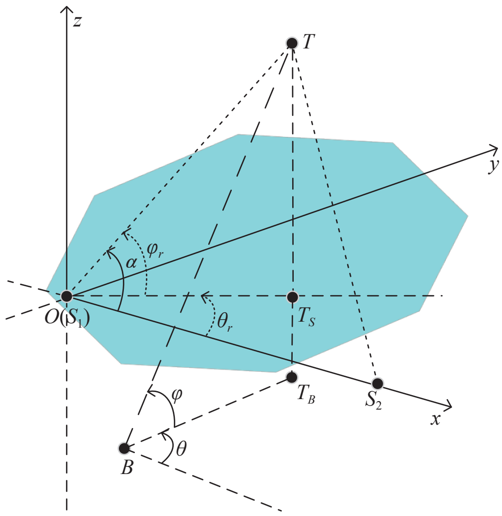

Fig. 2 IRS-aided DOA estimation geometric model

3.2 Elliptic parameters calculation

Consider a complete link, that is, a detection signal begins from the transmitter and then arrives at the receiver via IRS_1-target-IRS_2 link. By measuring the time difference, we can calculate the corresponding distance d of the link. Then, the sum of the distance between the target T and the two IRSs is

$$d_{S_1TS_2}=|\mathbf{S}_1\mathbf{T}|+|\mathbf{S}_2\mathbf{T}|=d-d_{B2S_1}-d_{B2S_2} \tag{7}$$

where $|\mathbf{S}_1\mathbf{T}|$ and $|\mathbf{S}_2\mathbf{T}|$ denote the modules of the vector $\mathbf{S}_1\mathbf{T}$ and $\mathbf{S}_2\mathbf{T}$, respectively. Especially, the d_{B2S_1} and d_{B2S_2} can be determined via the locations of the antenna array and two IRSs.

As shown in Fig. 2, S_1 and S_2 are the positions of the two IRSs, which can be considered as fixed points. The sum of the distance from T to S_1 and S_2 is a constant value $d_{S_1TS_2}$. Therefore, the trajectory of potential T is an ellipse with S_1 and S_2 as the focus, where the major axis length is $d_{S_1TS_2}$ and the focal length is $d_{S_12S_2}$.

We define the ellipse as $C(a,b,c)$, where a, b, and c represent the major semi-axis, minor semi-axis, and semi-focal length, respectively. The parameters a and c can be calculated as

$$\begin{cases} a=\dfrac{d_{S_1TS_2}}{2} \\ c=\dfrac{|\mathbf{S}_1\mathbf{S}_2|}{2}=\dfrac{d_{S_12S_2}}{2} \end{cases}. \tag{8}$$

Referring to the S_1TS_2 plane shown in Fig. 2, we establish a Cartesian coordinate system for the $S_{w_1}T_wS_{w_2}$ plane, which is illustrated in Fig. 3. In the Cartesian coordinate system, the coordinates of the target is $T_w(X_T,W_T)$, while the coordinates of point S_{w_1} and S_{w_2} are $(0,0)$ and $(2c,0)$, respectively. According to the relationship between the parameters of the ellipse, we obtain the minor semi-axis b:

$$b=\sqrt{a^2-c^2}. \tag{9}$$

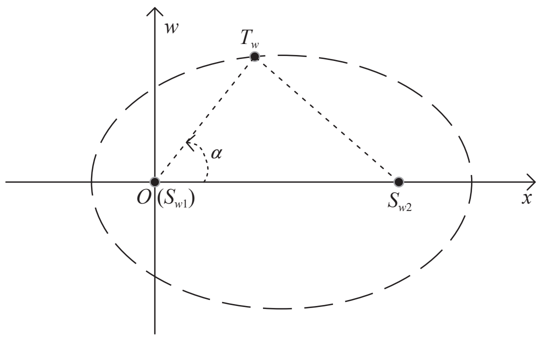

Fig. 3 IRS-aided DOA estimation ellipse model

Then, the equation of ellipse $C(a,b,c)$ is

$$\frac{(x-c)^2}{a^2}+\frac{w^2}{b^2}=1. \tag{10}$$

3.3 S_1T equation calculation

The azimuth angle θ_r and the elevation angle φ_r from IRS_1 to the target T can be known based on the characteristics of the IRS. The angle α between the vector $\mathbf{S}_1\mathbf{T}$ and the x-axis in Fig. 2 is the same as the angle between the vector $\mathbf{S}_{w_1}\mathbf{T}_w$ and the vector $\mathbf{S}_{w_1}\mathbf{S}_{w_2}$ in Fig. 3. Additionally, α can be represented by θ_r and φ_r:

$$\alpha=\arccos\frac{\boldsymbol{e}_x\cdot\boldsymbol{l}}{|\boldsymbol{e}_x||\boldsymbol{l}|}=\arccos(\cos\theta_r\cos\varphi_r) \tag{11}$$

where $\boldsymbol{e}_x=(1,0,0)$ is the unite vector of the vector $\mathbf{S}_1\mathbf{S}_2$. As shown in Fig. 2, there exists a non-zero vector $\boldsymbol{l}=(\cos\theta_r\cos\varphi_r,\sin\theta_r\cos\varphi_r,\sin\varphi_r)$, such that $\mathbf{S}_1\mathbf{T}=k\boldsymbol{l}$, where k is a non-zero constant. Subsequently, we derive the equation of $\boldsymbol{S}_{w_1}\boldsymbol{T}_w$:

$$w=x\cdot\tan\alpha. \tag{12}$$

3.4 Target coordinates calculation

Combining (10), (11), and (12), we derive the coordinates of point T_w, as shown in Fig. 2, where $T_w(X_T,W_T)$ can be sought using the "solve" function. It is worth mentioning that the distance R_{S_12T} between T and S_1 remains equal to the distance between T_w and S_{w1}. Therefore, we can use the coordinates of T_w to calculate the distance R_{S_12T} as

$$R_{S_12T} = |\mathbf{S}_1\mathbf{T}| = |\mathbf{S}_{w_1}\mathbf{T}_w| = \sqrt{X_T^2 + W_T^2}. \tag{13}$$

Then, the z-coordinate Z_T of the target T in the 3D Cartesian coordinate system is represented as

$$Z_T = R_{S_12T}\sin\varphi_r. \tag{14}$$

In the S_1TT_S plane, as shown in Fig. 2, the distance $R_{S_12T_S}$ from S_1 to T_S is expressed as

$$R_{S_12T_S} = |\mathbf{S}_1\mathbf{T}_S| = R_{S_12T}\cos\varphi_r \tag{15}$$

where $T_S(X_T, Y_T, 0)$ represents the projection point of T onto the XOY plane.

From Fig. 2, we can obtain the x-coordinate X_T and y-coordinate Y_T of T_S by using the geometric relationship:

$$\begin{cases} X_T = R_{S_12T_S}\cos\theta_r = R_{S_12T}\cos\varphi_r\cos\theta_r \\ Y_T = R_{S_12T_S}\sin\theta_r = R_{S_12T}\cos\varphi_r\sin\theta_r \end{cases}. \tag{16}$$

Finally, we attain the coordinate of the target, that is, $T(X_T, Y_T, Z_T)$.

3.5 DOA calculation

As shown in Fig. 2, according to spatial geometric relationships, the azimuth $\hat{\theta}$ of the receiver to target is equivalent to the angle formed between the vector $\mathbf{BT}_B$ and the positive direction of the x-axis. It is expressed as

$$\hat{\theta} = \arccos\frac{\boldsymbol{e}_x \cdot \mathbf{BT}_B}{|\boldsymbol{e}_x||\mathbf{BT}_B|} = \arccos\left(\frac{X_T - X_B}{|\mathbf{BT}_B|}\right). \tag{17}$$

where, $\mathbf{BT}_B = (X_T - X_B, Y_T - Y_B, 0)$ and $T_B(X_T, Y_T, Z_B)$ is the projection point of T onto the horizontal plane, where point B is located.

In the BTT_B plane, as shown in Fig. 2, the elevation angle $\hat{\varphi}$ from the receiver to the target is given by

$$\hat{\varphi} = \arctan\left(\frac{|\mathbf{T}_B\mathbf{T}|}{|\mathbf{BT}_B|}\right) = \arctan\left(\frac{|Z_T - Z_B|}{|\mathbf{BT}_B|}\right) \tag{18}$$

where $\mathbf{T}_B\mathbf{T} = (0, 0, Z_T - Z_B)$.

According to the above-mentioned description, the computational complexity of Algorithm 1 is $O(1)$.

Algorithm 1 The proposed algorithm

Require: Elliptic parameters a and c, the AOD of IRS$_1$ (θ_r, φ_r), and the coordinates of the antenna array, two IRSs $B(X_B, Y_B, Z_B)$, $S_1(0,0,0)$, and $S_2(2c,0,0)$, respectively.

Initialize: Establish the Cartesian coordinate system

(i) Calculate elliptic equation (10) via (8), and (9).

(ii) Calculate $\mathbf{S}_1\mathbf{T}$ equation (12) via (11).

(iii) Calculate the coordinate of target T via (14) and (16).

(iv) Calculate the DOA of target T via (17) and (18).

Ensure: $(\hat{\theta}, \hat{\varphi})$

4. Multi-pair-IRSs aided DOA estimation

In this section, we propose a multi-pair-IRSs aided 2D-DOA estimation for NLOS sources to improve the accuracy or expand the range of DOA estimation.

As shown in Fig. 1, if the target is out of the reflection range of IRS$_2$, the one-pair-IRSs framework will not work. Therefore, there is a limitation of the one-pair-IRSs aided DOA estimation framework, that is, the target must be in the detection zone of the IRS$_2$ (the IRS of reflecting detection signal from the target).

To extend the detection area of DOA estimation, we adopt a multi-pair-IRSs structure, where the IRS$_1$ is utilized to reflect the detection signal from the transmitter, and IRS$_m$ is used to reflect the detection signal from the target, as shown in Fig. 4(a). For convenience, we assume that all IRSs are deployed on the same plane, and they are collinear within this plane. In practice, IRSs can be arranged on different planes and our method still works. As shown in Fig. 4(a), if a target is between the IRS$_2$ and IRS$_3$, the target is in the reflection zone of the IRS$_3$, but out of the IRS$_2$. The target-IRS$_2$-BS link is not present, but we can use the target-IRS$_m$-BS ($m > 2$) link to establish the proposed framework and devise the DOA estimation. In this paper, we assume that all the pair-IRSs serve and thus M is calculated as

$$M = m - 1 \tag{19}$$

where the M denotes the number of the pair-IRSs that is to detect the target.

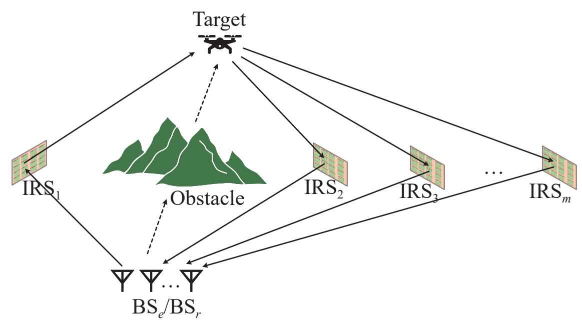

(a) Multi-pair-IRSs framework

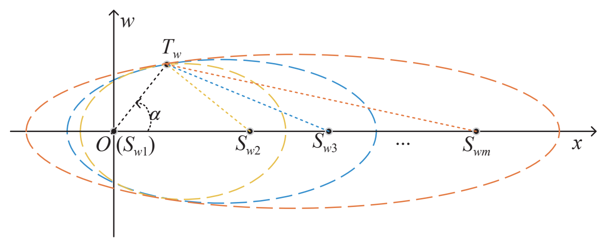

(b) Multi-pair-IRSs ellipse model

Fig. 4 Multi-IRSs aided DOA estimation framework

Moreover, we explore the impact of IRS deployment on the precision of DOA estimation. Therefore, we should consider the impact of the parameters a_j and c_j ($j \leqslant M$) on the precision of DOA estimation, where a_j and c_j correspond to the major semi-axis and semi-focal length of the jth pair-IRSs. To investigate the effect of a_j and c_j on DOA estimation, we use the eccentricity e_j of each ellipse as a measurement, that is, e can show the relationship between the IRS deployment and the accuracy of DOA estimation. The definition of e_j is as follows:

$$e_j = \frac{c_j}{a_j}. \tag{20}$$

According to the above analysis, each pair-IRSs can give a preliminary estimated DOA and the corresponding e_j can also be calculated. Based on their relationship, we design the weights for the DOA of each pair-IRSs using

$$w_{\theta_j} = \begin{cases} 1, & e_j \text{ is the minimum of } E \\ 0, & \text{otherwise} \end{cases} \tag{21a}$$

$$w_{\varphi_j} = \begin{cases} 1, & e_j \text{ is the maximum of } E \\ 0, & \text{otherwise} \end{cases} \tag{21b}$$

where $E = \{e_1, e_2, \cdots, e_M\}$, and $e_j \in E$ ($j \leqslant M$) represents the eccentricity corresponding to the ellipse formed by the jth pair-IRSs. w_{θ_j} and w_{φ_j} are the weight for the estimated azimuth and elevation angle of the jth pair-IRSs, respectively.

Then, the final DOAs result $\hat{\theta}_f$ and $\hat{\varphi}_f$ of the target are depended on the weighted average of the preliminary estimated positions of M pairs given by

$$\begin{cases} \hat{\theta}_f = \sum\limits_{j=1}^{M} w_{\theta_j} \hat{\theta}_j \\ \hat{\varphi}_f = \sum\limits_{j=1}^{M} w_{\varphi_j} \hat{\varphi}_j \end{cases} \tag{21}$$

where $\hat{\theta}_j$ and $\hat{\varphi}_j$ are the estimated azimuth and elevation angle of the jth pair-IRSs, respectively. The summary of the proposed BW method is given in Algorithm 2. Finally, it is not difficult to obtain that its computational complexity is $O(M)$.

Algorithm 2 The BW method

Require: Elliptic parameters of each pair a_j and c_j, the number of pair-IRSs M, and the DOA from BS to target of each group $(\hat{\theta}_j, \hat{\varphi}_j)$.

Initialize: Derive $(\hat{\theta}_j, \hat{\varphi}_j)$ of each pair

(i) Calculate the eccentricity e of each pair of ellipses via (20)

(ii) Calculate the number of pair-IRSs M via (19)

(iii) Calculate the weight w_{θ_j} and w_{φ_j} via (21a) and (21b)

(iv) Calculate the final DOA of target T via (22a) and (22b)

Ensure: $(\hat{\theta}_f, \hat{\varphi}_f)$

5. Numerical simulations

In this section, we evaluate the suggested method using synthetic data. All simulations are implemented on a computer with 13th Gen Inter(R) Core(TM) i9-13900K 3.0 GHz CPU and 32 GB memory.

5.1 Simulation setting

In the experiment, the parameters are configured as $B(200, -400, -30)$, $S_1(0,0,0)$, and $S_m(2c, 0, 0)$ ($m \geqslant 2$). It is worth pointing out that the coordinates of B and S_1 are unchanged in the subsequent experiments. We use $(\bar{\theta}, \bar{\varphi})$ and $(\bar{\theta}_r, \bar{\varphi}_r)$ to denote the true angles from the antenna array to the target and the true angles from IRS_1 to the target, respectively. To evaluate the impact of (θ_r, φ_r) on estimation performance, we introduce perturbations $(\Delta\theta, \Delta\varphi)$ to $(\bar{\theta}_r, \bar{\varphi}_r)$, resulting in $(\bar{\theta}_r + \Delta\theta, \bar{\varphi}_r + \Delta\varphi)$.

In Experiment 2 and Experiment 3, we investigate the impact of the number of pair-IRSs M and perturbations $\varDelta$ on DOA estimation, where the mean method and the BW method with multi-pair-IRSs structures are compared. The definition of the mean method is

$$\begin{cases} \hat{\theta}_{m_f} = \dfrac{1}{M} \sum\limits_{j=1}^{M} \hat{\theta}_j \\ \hat{\varphi}_{m_f} = \dfrac{1}{M} \sum\limits_{j=1}^{M} \hat{\varphi}_j \end{cases} \tag{22}$$

where $\hat{\theta}_j$ and $\hat{\varphi}_j$ are the estimated azimuth and elevation angle of the jth pair-IRSs combination, respectively.

In this paper, the performance of DOA estimation is measured using mean absolute error (MAE), defined as

$$\begin{cases} \text{MAE}_\theta = \dfrac{|\hat{\theta}_{f_+} - \bar{\theta}| + |\hat{\theta}_{f_-} - \bar{\theta}|}{2} \\ \text{MAE}_\varphi = \dfrac{|\hat{\varphi}_{f_+} - \bar{\varphi}| + |\hat{\varphi}_{f_-} - \bar{\varphi}|}{2} \end{cases} \tag{23}$$

where $\hat{\theta}_{f_+}$ ($\hat{\theta}_{f_-}$) and $\hat{\varphi}_{f_+}$ ($\hat{\varphi}_{f_-}$) represent the estimates of θ_f and φ_f, respectively, with positive (negative) perturbations.

5.2 Estimation performance

Experiment 1 In this experiment, we investigate the impact of e on the estimation precision. The coordinate of target is $T(500, 1\,000, 1\,500)$. Then, we calculate $(\bar{\theta}, \bar{\varphi}) = (77.91°, 46.90°)$ and $(\bar{\theta}_r, \bar{\varphi}_r) = (63.43°, 53.30°)$.

The system parameter c is set as $c \in [400, 4\,000]$ m in 100 m increments, and the value of e ranges from 0.21 to 0.84. Note that the second IRS is located at $S_2(2c, 0, 0)$, and we obtain the coordinate of IRS_2, that is, $(800, 0, 0)$. The perturbations added to θ_r and φ_r are $1°$. As shown in Fig. 5(a), the trend of MAE_θ illustrates an improving trend as e increases, while the trend of MAE_φ is the opposite, as shown in Fig. 5(b). From Fig. 5, we know the MAE_θ is less as the e is small. However, the MAE_φ is the opposite. Therefore, we design the BW method in Section 4.

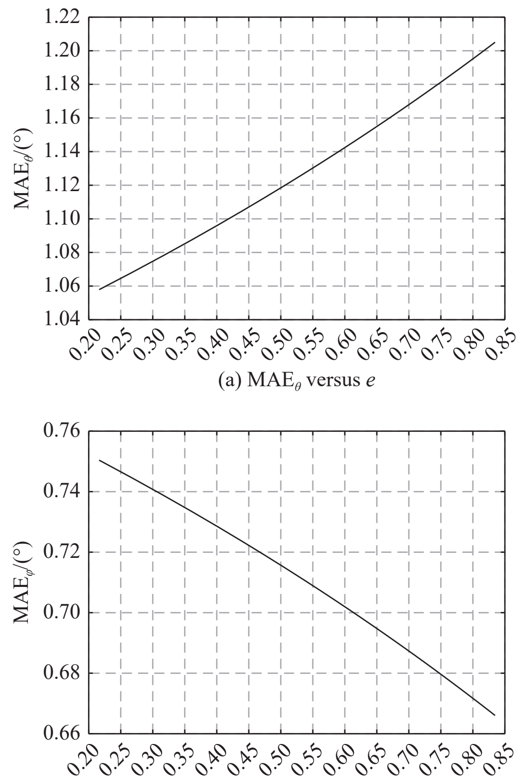

(a) MAE_θ versus e

(b) MAE_φ versus e

Fig. 5 MAE_θ and MAE_φ versus e with $\Delta = 1°$

Experiment 2 We study the impact of the parameter M on the accuracy of DOA estimation, and compare the mean and BW methods on the DOA estimation performance. In this experiment, the coordinate of target is set as $T(380, 540, 230)$, and then we calculate $(\bar{\theta}, \bar{\varphi}) = (79.16°, 15.20°)$ and $(\bar{\theta}_r, \bar{\varphi}_r) = (54.87°, 19.20°)$. The parameter M is set from 1 to 10, and the selection of c of multi-pair-IRSs is $\{2\,200, 2\,000, 1\,800, 1\,600, 1\,400, 1\,200, 1\,000, 800, 600, 400\}$ m. Subsequently, it is easy to obtain the coordinate of the qth IRS_2 $(q = 1, 2, \cdots, M)$. For example, the first location of IRS_2 is $S_2 = (4\,400, 0, 0)$, where the corresponding $q = 1$. Fig. 6(a) illustrates the impact of M on the MAE_θ. It is seen that the MAE_θ of BW and mean show a decreasing trend as the parameter M increases. In addition, the BW method outperforms the mean algorithm. In Fig. 6(b), we observe that the BW approach outperforms the mean manner. However, the MAE_φ with BW method is a constant, and that with mean manner increases with M increasing. This is because we use the result of Experiment 1 to design the weight of the BW method for $\hat{\varphi}$. As shown in Fig. 5(b), the MAE_φ is the minimum when the e_j is the maximum. Therefore, we use the $\hat{\varphi}_j$ of the jth pair-IRSs, whose e_j is the maximum of E, to be the final elevation angle $\hat{\varphi}_f$. Note that the parameter c is set as a decreasing trend in Experiment 2.

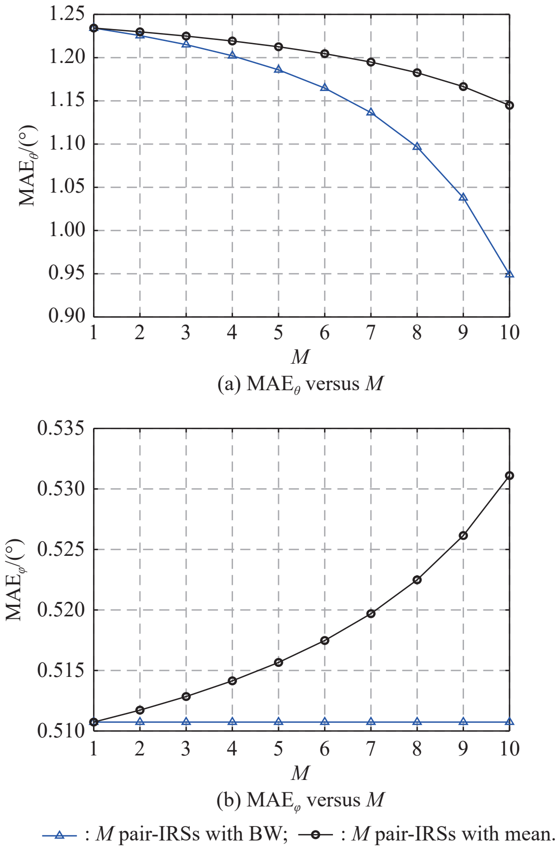

(a) MAE_θ versus M

(b) MAE_φ versus M

Fig. 6 MAE_θ and MAE_φ versus M with Δ=1°

Experiment 3 We compare the performance of mean and BW methods on the estimation accuracy with perturbations. In this simulation, we use five pair-IRSs ($M = 5$) to aid 2D-DOA estimation, and the parameter c of multi-pair-IRSs is set as $c \in C$, where $C = \{1\,200, 1\,000, 800, 600, 400\}$ m. Then, it is easy to derive the coordinate of IRS_m $(m = 2, 3, 4, 5, 6)$, which is $(2C(l), 0, 0)$ $(l = 1, 2, \cdots, M)$. It is worth mentioning that the parameter c for one-pair-IRSs is set as 800 m and the location of target is $T(700, 1\,200, 1\,400)$, leading to $(\bar{\theta}, \bar{\varphi}) = (72.65°, 40.47°)$

and $(\bar{\theta}_r, \bar{\varphi}_r) = (59.74°, 45.22°)$.

Fig. 7 illustrates the impact of $\Delta\theta$ on MAE_θ and MAE_φ with $\Delta\varphi = 1°$ and $\Delta\theta \in [-2.5°, 2.5°]$. It is seen from Fig. 7(a) that the BW method is better than the mean manner in MAE_θ. Besides, we see that the accuracy of DOA estimation of multi-pair-IRSs structure is higher than that of the one-pair-IRSs. In particular, the MAE_θ of the BW method is less than that of the one-pair-IRSs and multi-pair-IRSs framework using the mean method. As shown in Fig. 7(b), we see that MAE_φ shows a decreasing trend as $\Delta\theta$ increases, with the multi-pair-IRSs architecture or one-pair-IRSs structure. Notably, the MAE_φ of the BW method is lower than those of the other two methods.

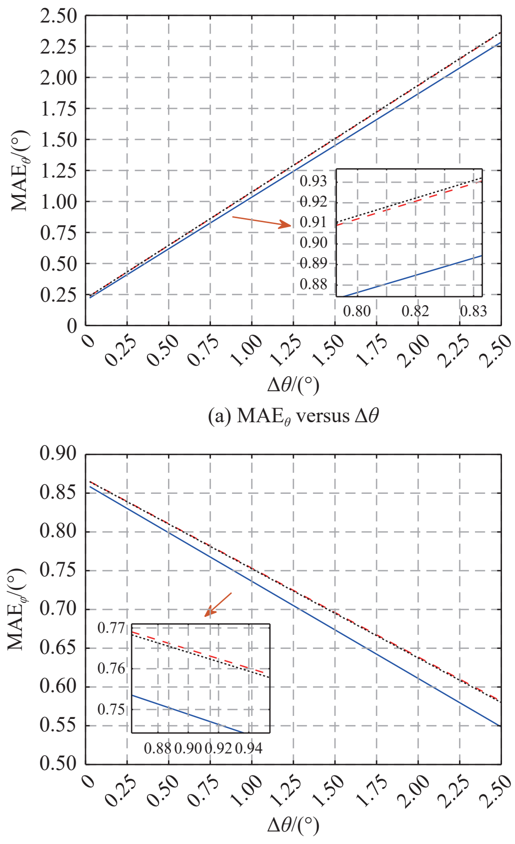

(a) MAE_θ versus $\Delta\theta$

(b) MAE_φ versus $\Delta\theta$

—— : Five pair-IRSs with BW; - - - : Five pair-IRSs with mean; ······· : One pair-IRSs.

Fig. 7 MAE_θ and MAE_φ versus $\Delta\theta$ with $\Delta\varphi = 1°$ and $M = 5$

Fig. 8 shows the effect of $\Delta\varphi$ on MAE_θ and MAE_φ, where $\Delta\theta$ is set to $1°$, and $\Delta\varphi$ ranges from $-2.5°$ to $2.5°$. As seen in Fig. 8(a), the MAE_θ grows with the increase of $\Delta\varphi$, and the BW method outperforms the other two methods in terms of MAE_θ. Fig. 8(b) illustrates that the BW method performs better on MAE_φ than the other two methods. Both one-pair-IRSs and multi-pair-IRSs with the mean method, show a decrease in MAE_φ with $\Delta\varphi$ ranging from $0°$ to $0.125°$. The BW method is still a decreasing trend in the following short range. However, all the methods show an increasing trend of MAE_φ as $\Delta\varphi$ is from $0.14°$ to $2.5°$. In the latter range, the BW method is better than other methods on the MAE_φ.

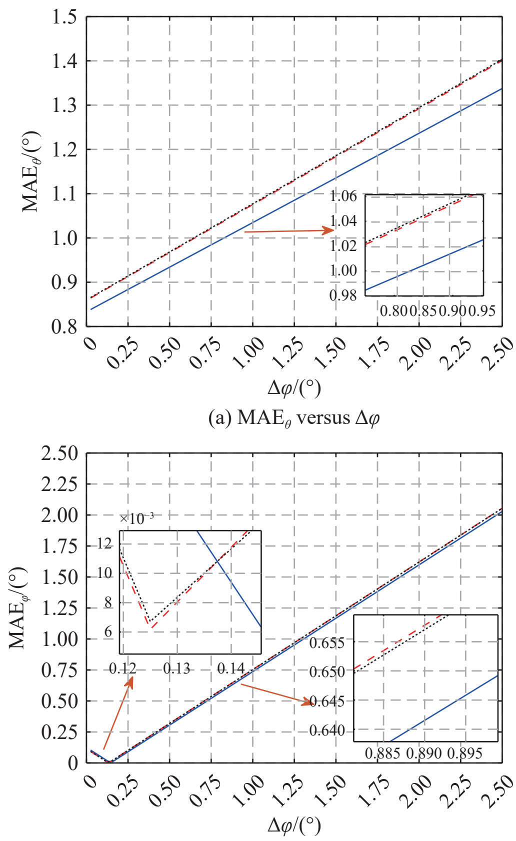

(a) MAE_θ versus $\Delta\varphi$

(b) MAE_φ versus $\Delta\varphi$

—— : Five pair-IRSs with BW; - - - : Five pair-IRSs with mean; ······· : One pair-IRSs.

Fig. 8 MAE_θ and MAE_φ versus $\Delta\varphi$ with $\Delta\theta = 1°$ and $M = 5$

Furthermore, both Fig. 7 and Fig. 8, show that the MAE_θ or MAE_φ of the one-pair-IRSs and multi-pair-IRSs with the mean method reveal a slight performance gap. Compared to the former two approaches, the MAE of the multi-pair-IRSs with the BW method is less.

Experiment 4 In this experiment, parameters c and M of multi-pair-IRSs are set the same as Experiment 3, where $\Delta\theta \in [-2.5°, 2.5°]$ and $\Delta\varphi \in [-2.5°, 2.5°]$. The coordinate of target is $T(400, 1\,200, 300)$, from which the angles $(\bar{\theta}, \bar{\varphi}) = (82.88°, 11.57°)$ and $(\bar{\theta}_r, \bar{\varphi}_r) = (71.57°, 13.34°)$ are calculated. Fig. 9 shows the impact of perturbations on the estimation performance with the BW method. As seen in Fig. 9(a), MAE_θ increases as $\Delta\theta$ and $\Delta\varphi$ enhance. However, $\Delta\theta$ has a greater impact on MAE_θ than $\Delta\varphi$. Fig. 9(b) shows that MAE_φ increases with $\Delta\varphi$.

Additionally, when $\Delta\varphi$ is small, MAE$_\varphi$ grows with $\Delta\theta$, while MAE$_\varphi$ decreases with $\Delta\theta$ when $\Delta\varphi$ is large. Furthermore, $\Delta\varphi$ has a greater impact on MAE$_\varphi$ than $\Delta\theta$.

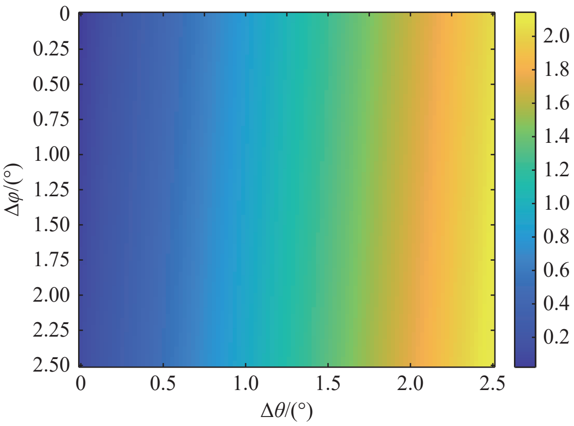

(a) MAE$_\theta$ versus $\Delta\varphi$ and $\Delta\theta$

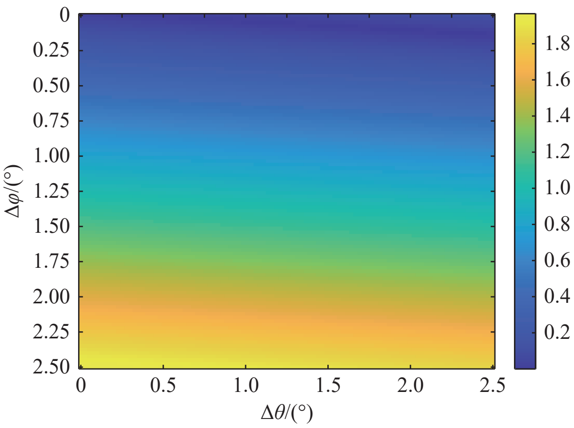

(b) MAEφ versus $\Delta\varphi$ and $\Delta\theta$

Fig. 9 MAE$_\theta$ and MAE$_\varphi$ versus Δ with $M = 5$

6. Conclusions

In this paper, we design an IRS-aided 2D-DOA estimation algorithm in NLOS environments. First, a 2D-DOA estimation framework in NLOS scenarios is proposed by utilizing IRS to change the radio wave propagation. Then, the EP technique is derived by combining the prior information of the antenna array and the position of the IRS. Furthermore, we derive a closed-form solution to seek for the target localization. Finally, the 2D-DOA of the target is obtained. Simulation results demonstrate the effectiveness of the proposed method for sensing target.

In addition, based on the proposed framework and algorithm, we design a multi-pair-IRSs architecture and a BW method to improve the accuracy of DOA estimation. We utilize the relation between the eccentricity e of the ellipse and MAE is used to design the weight. Compared with one-pair-IRSs and multi-pair-IRSs architecture with the mean method, the simulation results show that the multi-pair-IRSs architecture with the BW method can improve the accuracy of DOA. However, we do not consider the impact of multipath effects on this framework, which may affect the applicability of the algorithm. Additionally, we do not consider the interference arriving at the receiving antenna array, which may provide incorrect information for DOA estimation.

In the future, we will design the transmitting signal, such that the signal and interference can be distinguished. Nevertheless, the weights used need to be further optimized to achieve higher DOA estimation accuracy. Additionally, we will study the framework of IRS-aided 2D-DOA estimation for multi-targets in NLOS scenarios.

References

[1] KHABBAZIBASMENJ A, HASSANIEN A, VOROBYOV S A, et al. Efficient transmit beamspace design for search-free based DOA estimation in MIMO radar. IEEE Trans. on Signal Processing, 2014, 62(6): 1490–1500.

[2] GHELFI P, LAGHEZZA F, SCOTTI F, et al. A fully photonics-based coherent radar system. Nature, 2014, 507(7492): 341–345.

[3] SCHMIDT R. Multiple emitter location and signal parameter estimation. IEEE Trans. on Antennas and Propagation, 1986, 34(3): 276–280.

[4] RAO B D, HARI K V S. Performance analysis of root-MUSIC. IEEE Trans. on Acoustics, Speech, and Signal Processing, 1989, 37(12): 1939–1949.

[5] KUNDU D. Modified MUSIC algorithm for estimating DOA of signals. Signal Processing, 1996, 48(1): 85–90.

[6] LI X P, LIU Z, SHI Z L, et al. MUSIC with capped Frobenius norm: efficient robust direction-of-arrival estimator. IEEE Trans. on Aerospace and Electronic Systems, 2023, 59(6): 8090−8103.

[7] ZENG W J, SO H C, HUANG L. ℓ_p-MUSIC: robust direction-of-arrival estimator for impulsive noise environments. IEEE Trans. on Signal Processing, 2013, 61(17): 4296–4308.

[8] ROY R, KAILATH T. ESPRIT-estimation of signal parameters via rotational invariance techniques. IEEE Trans. on Acoustics, Speech, and Signal Processing, 1989, 37(7): 984–995.

[9] QIAN C, HUANG L, SIDIROPOULOS N D, et al. Enhanced PUMA for direction-of-arrival estimation and its performance analysis. IEEE Trans. on Signal Processing, 2016, 64(16): 4127–4137.

[10] ZHANG R, XIA W W, YAN F, et al. A single-site positioning method based on TOA and DOA estimation using virtual stations in NLOS environment. China Communications, 2019, 16(2): 146–159.

[11] GUVENC I, CHONG C C. A survey on TOA based wireless localization and NLOS mitigation techniques. IEEE Communications Surveys & Tutorials, 2009, 11(3): 107–124.

[12] CHAN Y T, TSUI W Y, SO H C, et al. Time-of-arrival based localization under NLOS conditions. IEEE Trans. on Vehicular Technology, 2006, 55(1): 17–24.

[13] MUIRHEAD D, IMRAN M A, ARSHAD K. A survey of the challenges, opportunities and use of multiple antennas in current and future 5G small cell base stations. IEEE Access, 2016, 4: 2952–2964.
[14] XU Z H, GUO S S, CHEN J H, et al. Multi-domain features based NLOS target localization method for MIMO UWB radar. IEEE Sensors Journal, 2023, 23(23): 29314−29322.
[15] BASAR E, DI RENZO M, DE ROSNY J, et al. Wireless communications through reconfigurable intelligent surfaces. IEEE Access, 2019, 7: 116753–116773.
[16] JIANG Z M, RIHAN M, ZHANG P, et al. Intelligent reflecting surface aided dual-function radar and communication system. IEEE Systems Journal, 2021, 16(1): 475–486.
[17] CHEN H Y, BAI Y C, WANG Q, et al. DOA estimation assisted by reconfigurable intelligent surfaces. IEEE Sensors Journal, 2023, 23(12): 13433–13442.
[18] WEN F Q, SHI J P, LIN Y, et al. Joint DOD and DOA estimation for NLOS target using IRS-aided bistatic MIMO radar. IEEE Trans. on Vehicular Technology, 2024, 73(10): 15798−15802.
[19] CHEN Z, TANG J, HUANG L, et al. Robust target positioning for reconfigurable intelligent surface assisted MIMO radar system. IEEE Trans. on Vehicular Technology, 2023, 72(11): 15098–15102.
[20] ZHANG G L, ZHANG D H, DENG H Y, et al. Practical passive indoor localization with intelligent reflecting surface. IEEE Trans. on Mobile Computing, 2024, 23(12): 12477–12490.
[21] ZHANG G L, ZHANG D H, HE Y, et al. Multi-person passive WiFi indoor localization with intelligent reflecting surface. IEEE Trans. on Wireless Communications, 2023, 22(10): 6534–6546.
[22] YANG L L, MENG F H, ZHANG J, et al. On the performance of RIS-assisted dual-hop UAV communication systems. IEEE Trans. on Vehicular Technology, 2020, 69(9): 10385–10390.
[23] HUA M, YANG L X, WU Q Q, et al. UAV-assisted intelligent reflecting surface symbiotic radio system. IEEE Trans. on Wireless Communications, 2021, 20(9): 5769–5785.
[24] CHEN P, CHEN Z M, ZHENG B X, et al. Efficient DOA estimation method for reconfigurable intelligent surfaces aided UAV swarm. IEEE Trans. on Signal Processing, 2022, 70: 743–755.
[25] SWINDLEHURST A L, ZHOU G, LIU R, et al. Channel estimation with reconfigurable intelligent surfaces-a general framework. Proceedings of the IEEE, 2022, 110(9): 1312–1338.
[26] JEONG S, FARHANG A, PEROVIC N S, et al. Low-complexity joint CFO and channel estimation for RIS-aided OFDM systems. IEEE Wireless Communications Letters, 2021, 11(1): 203–207.
[27] DE ARAÚJODE G T, DE ALMEIDA A L F, BOYER R. Channel estimation for intelligent reflecting surface assisted MIMO systems: a tensor modeling approach. IEEE Journal of Selected Topics in Signal Processing, 2021, 15(3): 789–802.
[28] DI RENZO M, ZAPPONE A, DEBBAH M, et al. Smart radio environments empowered by reconfigurable intelligent surfaces: how it works, state of research, and the road ahead. IEEE Journal on Selected Areas in Communications, 2020, 38(11): 2450–2525.
[29] LIU Y W, LIU X, MU X D, et al. Reconfigurable intelligent surfaces: principles and opportunities. IEEE Communications Surveys & Tutorials, 2021, 23(3): 1546–1577.
[30] WU Q Q, ZHANG R. Towards smart and reconfigurable environment: intelligent reflecting surface aided wireless network. IEEE Communications Magazine, 2019, 58(1): 106–112.
[31] GONG S, LU X, HOANG D T, et al. Toward smart wireless communications via intelligent reflecting surfaces: a contemporary survey. IEEE Communications Surveys & Tutorials, 2020, 22(4): 2283–2314.
[32] HUANG C, ZAPPONE A, ALEXANDROPOULOS G C, et al. Reconfigurable intelligent surfaces for energy efficiency in wireless communication. IEEE Trans. on Wireless Communications, 2019, 18(8): 4157–4170.
[33] ZHANG Z J, DAI L L, CHEN X B, et al. Active RIS vs. passive RIS: which will prevail in 6G? IEEE Trans. on Communications, 2022, 71(3): 1707–1725.
[34] BASAR E. Reconfigurable intelligent surface-based index modulation: a new beyond MIMO paradigm for 6G. IEEE Trans. on Communications, 2020, 68(5): 3187–3196.
[35] HUA M, WU Q Q, CHEN W, et al. Intelligent reflecting surface assisted localization: performance analysis and algorithm design. IEEE Wireless Communications Letters, 2024, 13(1): 84−88.
[36] HUA M, CHEN G J, MENG K T, et al. 3D multi-target localization via intelligent reflecting surface: protocol and analysis. IEEE Trans. on Wireless Communications, 2024, 23(11): 16527−16543.
[37] WEN F Q, WANG H, GUI G, et al. Polarized intelligent reflecting surface aided 2D-DOA estimation for NLOS sources. IEEE Trans. on Wireless Communications, 2024, 23(7): 8085−8098.
[38] XIONG W X, CHENG G, SCHINDELHAUER C, et al. Robust matrix completion for elliptic positioning in the presence of outliers and missing data. IEEE Trans. on Geoscience and Remote Sensing, 2023, 61: 5105912.
[39] ÖZDOGAN Ö, BJÖRNSON E, LARSSON E G. Intelligent reflecting surfaces: physics, propagation, and pathloss modeling. IEEE Wireless Communications Letters, 2019, 9(5): 581–585.
[40] PAN C H, ZHOU G, ZHI K D, et al. An overview of signal processing techniques for RIS/IRS-aided wireless systems. IEEE Journal of Selected Topics in Signal Processing, 2022, 16(5): 883–917.
[41] YANG L, YANG J X, XIE W W, et al. Secrecy performance analysis of RIS-aided wireless communication systems. IEEE Trans. on Vehicular Technology, 2020, 69(10): 12296–12300.
[42] WANG J L, FANG J, LI H B, et al. Intelligent reflecting surface-assisted NLOS sensing with OFDM signals. IEEE Trans. on Signal Processing, 2024, 72: 5322–5337.
[43] RUI L, HO K C. Elliptic localization: performance study and optimum receiver placement. IEEE Trans. on Signal Processing, 2014, 62(18): 4673–4688.

Biographies

DUAN Min was born in 2000. He received his B.E. degree in communications engineering from Dalian University, Dalian, China, in 2022. He is currently pursuing his M.S. degree with the College of Electronics and Information Engineering, Shenzhen University, Shenzhen, China. His research interests include direction of arrival (DOA) estimation, target localization, and intelligent reflecting surface.
E-mail: 2310433033@email.szu.edu.cn

LI Xiaopeng was born in 1991. He received his B.E. degree in electronic science and technology from Yanshan University, Qinhuangdao, China, in 2015, M.S. degree in electronic information engineering, and Ph.D. degree in electrical engineering from City University of Hong Kong, Hong Kong SAR, China, in 2018 and 2022, respectively. He was a research assistant with the Department of Information Engineering, Shenzhen University, Shenzhen, China from 2018 to 2019, and a postdoctoral fellow with the Department of Electrical Engineering, City University of Hong Kong from 2022 to 2023. He is currently an assistant professor with the College of Electronics and Information Engineering, Shenzhen University. His research interests include robust signal processing, sparse recovery, matrix processing, tensor processing, optimization methods, machine learning, and their applications in various areas of engineering, including target estimation, image recovery, video restoration, hyperspectral unmixing, and stock market analysis.
E-mail: x.p.li@szu.edu.cn

HUANG Lei was born in 1975. He received his B.S. and Ph.D. degrees in electronic engineering from Xidian University, Xi'an, China, in 2000 and 2005, respectively. He is currently with the College of Electronics and Information Engineering, Shenzhen University, as a chair professor, and established the Shenzhen Key Laboratory of Advanced Navigation Technology as the founding director. He is now the executive dean of the College of Electronics and Information Engineering and the executive director of the State Key Laboratory of Radio Frequency Heterogeneous Integration, Shenzhen University. His research interests include spectral estimation, array signal processing, statistical signal processing, and their applications in radar, navigation and wireless communications.
E-mail: lhuang@szu.edu.cn

HUA Meng was born in 1991. He received his Ph.D. degree from the School of Information Science and Engineering, Southeast University, Nanjing, China, in 2021. He was the recipient of the Outstanding Ph.D. Thesis Award of Chinese Institute of Electronics in 2021. From January 2021 to June 2023, he was a postdoc at University of Macau. From June 2023 to January 2024, he was a postdoc at City University of Hong Kong. From January 2024, he has been a research associate at Imperial College London. He is an associate editor of the IEEE Transactions on Communications and IEEE Open Journal of the Communications Society. His current research interests include 6G-goal artificial intelligence (AI), localization, integrated sensing and communication, and intelligent reflecting surface-assisted communication.
E-mail: m.hua@imperial.ac.uk

LI Qiang was born in 1987. He received his Ph.D. degree in navigation guidance and control from Harbin Engineering University, China, in 2015. From 2015 to 2018, he was a postdoctoral researcher with the College of Electronics and Information Engineering, Shenzhen University. He joined communication group of the University of Sheffield, UK, in 2016, as a visiting scholar, where he researched the phase retrieval algorithms for antennaarray. He is currently an assistant professor with the College of Electronics and Information Engineering, Shenzhen University. His research interests include array signal processing, satellite navigation, and signal recovery algorithms.
E-mail: liqiang@szu.edu.cn